# Bond connectivity measured via relaxation-assisted two-dimensional infrared spectroscopy

Sri Ram G. Naraharisetty, Valeriy M. Kasyanenko, and Igor V. Rubtsov<sup>a)</sup>
Department of Chemistry, Tulane University, New Orleans, Louisiana 70118, USA

(Received 19 October 2007; accepted 17 January 2008; published online 11 March 2008)

The relaxation-assisted two-dimensional infrared (RA 2DIR) method is a novel technique for probing structures of molecules, which relies on vibrational energy transport in molecules. In this article we demonstrate the ability of RA 2DIR to detect the bond connectivity patterns in molecules using two parameters, a characteristic intermode energy transport time (arrival time) and a cross-peak amplification coefficient. A correlation of the arrival time with the distance between the modes is demonstrated. An 18-fold amplification of the cross-peak amplitude for the modes separated by ~11 Å is shown using RA 2DIR; larger cross-peak amplifications are expected for the modes separated by larger distances. The RA 2DIR method enhances the applicability of 2DIR spectroscopy by making practical the long-range measurements using a variety of structural reporters, including weak IR modes. The data presented demonstrate the analytical power of RA 2DIR which permits the speedy structural assessments of the bond connectivity patterns. © 2008 American Institute of Physics. [DOI: 10.1063/1.2842071]

#### INTRODUCTION

Development of new methods for determining threedimensional structures of molecules in solution at physiological temperatures is an important challenge of modern science. In the last decade two-dimensional infrared (2DIR) spectroscopy has demonstrated widely its capabilities of measuring structural constraints for molecules in solution at ambient temperatures. <sup>1–16</sup> The method measures pairwise interactions of vibrational modes and has clear similarities with the nuclear Overhauser effect spectroscopy (NOESY) method of 2D NMR spectroscopy. 17,18 Interactions among modes of the same type have been extensively used to measure structural constraints. 1-10 More recently, the analogs of heteronuclear 2D NMR have been developed where interactions of vibrational modes of different types and having very different frequencies were used to obtain structural information. 11-15 The IR modes with large transition dipole, such as C=O, C-N, N-H, and O-H, were dominantly used as 2DIR structural reporters. 1-10 Such strong IR modes, however, are often abundant in molecules, and especially abundant in biopolymers, which complicates their use as structural reporters in such molecules. Weak IR modes, which are readily available, can potentially deliver large sets of structural constraints and permit selecting mode pairs convenient for structural measurements in specific conditions. Therefore, implementation of weak IR modes as 2DIR structural reporters is very attractive in spite of experimental difficulties caused by small transition dipoles of such modes. Several examples of the cross-peak measurements using interactions of strong and weak modes 13,15 and interactions of two weak modes<sup>19</sup> have been demonstrated. In all these examples, the modes used as reporters were separated by less

than 2-3 Å. Because the cross-peak amplitude decreases steeply with the distance increase, it is difficult to use weak modes separated by larger distances as structural reporters.

We have recently proposed and tested a novel approach in 2DIR spectroscopy, the relaxation-assisted 2DIR (RA 2DIR) method, <sup>20,21</sup> which has similarities to the homonuclear total correlation spectroscopy (TOCSY) 2D NMR method and its heteronuclear counterpart, HMBC. Traditional 2DIR spectroscopy measures cross peaks that originate from the direct interaction (coupling) of vibrational modes [Fig. 1(a)]. The direct mode-to-mode coupling is manifested in a shift of the  $\omega_1$  and  $\omega_2$  combination band level,  $\Delta_{12}$  [Fig. 1(d)], which is called the off-diagonal anharmonicity and which can be linked to the distance between the interacting modes using theoretical modeling.<sup>22,23</sup> The RA 2DIR cross peaks rely on energy transport in molecules [Fig. 1(b)]. The energy of the initially excited mode,  $\omega_1$ , relaxes into other modes,  $\omega_x$ , via intramolecular vibrational energy redistribution process and the excess energy travels in the molecule in all directions in a cooling process [Fig. 1(b)]. If the probed mode,  $\omega_2$ , is at substantial distance from the initially excited mode,  $\omega_1$ , it takes time for the excess energy to reach the site where  $\omega_2$  is located [Fig. 1(b)]. Some lower-frequency modes,  $\omega_x$ , located near the  $\omega_2$  site, or the  $\omega_2$  itself, become excited when the excess energy reaches the site [Fig. 1(e)]. Because of large spatial overlap with  $\omega_2$ , these low-frequency modes  $(\omega_x)$  could be strongly coupled to  $\omega_2$ , resulting in a large value of the off-diagonal anharmonicity  $\Delta_{x2}$ . This coupling can produce 2DIR cross peaks which are stronger than the direct coupling cross peaks. In case the  $\omega_2$  mode itself is excited via energy transport from  $\omega_1$ , the diagonal anharmonicity of the  $\omega_2$  mode,  $\Delta_2$ , replaces the off-diagonal anharmonicity  $\Delta_{x2}$ . Using the dual-frequency RA 2DIR method we have recently demonstrated a sixfold increase in the C  $\equiv$ N/C $\equiv$ O cross-peak amplitude in 4-acetylbenzonitrile.<sup>21</sup>

a) Electronic mail: irubtsov@tulane.edu.

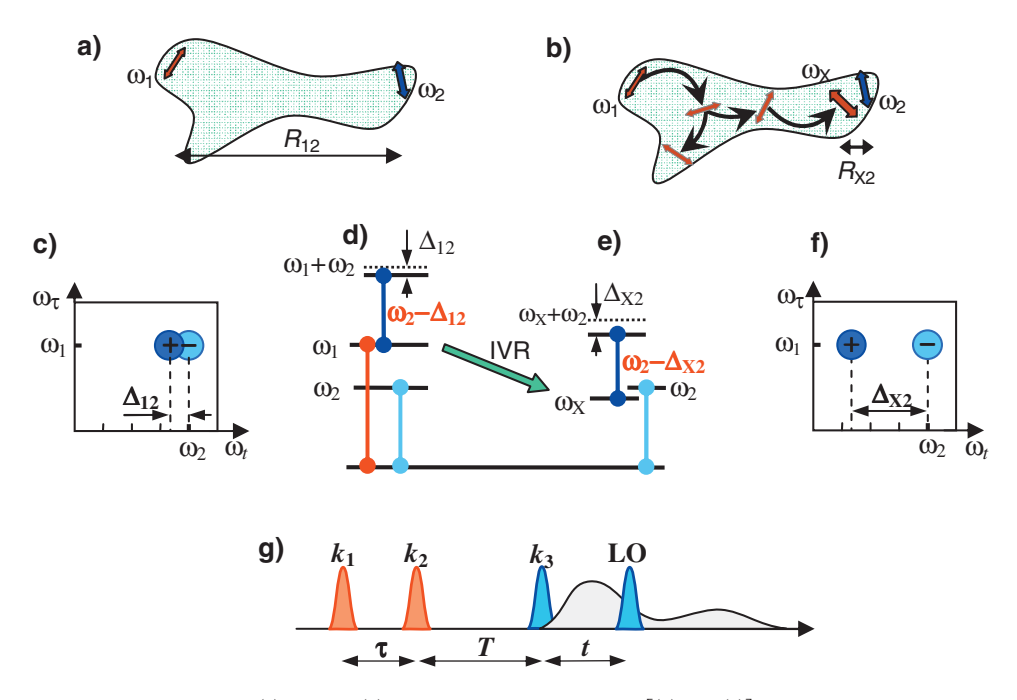


FIG. 1. (Color) Cartoons for the direct-coupling (a) and RA (b) cross peaks. Energy diagram [(d) and (e)] showing formation of the direct coupling [(c) and (d)] and RA cross peaks [(e) and (f)]. (g) The experimental pulse sequence for the dual-frequency measurements.

Note that the location of the RA cross peak in the 2DIR spectrum will be roughly at  $(\omega_2, \omega_1)$  frequencies [Fig. 1(f)], similarly to the direct coupling cross peak [Fig. 1(c)].

The amplitude of the RA 2DIR cross peaks depends on two main factors: The coupling strength of the  $\omega_2$  and  $\omega_x$ modes, which results in the shift of the (2+X) combination band,  $\Delta_{x2}$  [Fig. 1(e)], and the occupation number (that is the excited state population) for the X mode(s) achieved via energy transport. If  $\Delta_{x2} \gg \Delta_{12}$  the RA cross peaks could be stronger than the direct-coupling cross peaks, despite the small occupation numbers for the modes X. Clearly, the RA cross peaks reflect interactions that are different from the direct-coupling cross peaks resulting in a different type of structural information (vide infra). The angles between transition moments of vibrational modes can be measured using RA cross peaks in the same way as using the direct-coupling cross peaks.<sup>21</sup> In this article we demonstrate the capability of the RA 2DIR method in measuring the bond connectivity patterns in molecules in a way similar to that of the TOCSY and HMBC techniques of 2D NMR spectroscopy. These experiments expand the boundaries of 2DIR spectroscopy in accessing structural features of molecules and highlight the analytical power of the RA 2DIR method.

## **MATERIALS AND METHODS**

Sample preparation. The 2DIR and linear Fourier transform infrared experiments were performed using a 120 mM solution of 4-(4-oxo-piperidine-1-carbonyl)-benzonitrile (J & W PharmLab) (PBN) in chloroform (Aldrich) placed in a sample cell made of two CaF<sub>2</sub> wafers and a 50  $\mu$ m thick Teflon spacer. All experiments were performed at room temperature, 23.5 ± 0.7 °C.

Dual-frequency heterodyne 2DIR. Short pulses in the mid-IR spectral region, required for 2DIR experiments, were

produced using laser pulses of 804 nm wavelength and 44 fs duration generated by a Ti:sapphire oscillator and a regenerative amplifier system (Coherent Inc.). The output of the regenerative amplifier (900  $\mu$ J/pulse) was split into two equal parts to pump two in-house built optical parametric amplifiers, each equipped with a difference frequency generation (DFG) unit. Two independently tunable mid-IP pulse trains were generated by the two DFG modules that use 1.5 mm thick AgGaS<sub>2</sub> crystals ( $\theta$ =37.1°, Ekspla). The resulting pulses had energies of 1.8 and 2.5  $\mu$ J/pulse in the 6 and 4  $\mu$ m spectral regions, respectively, the duration of  $\sim$ 90 fs and the bandwidth of 176  $\pm$ 5 cm<sup>-1</sup> throughout the spectral region. More details of the dual-frequency heterodyned photon-echo setup can be found in Refs. 13 and 19.

Each mid-IR beam was split into two equal parts to provide  $k_1, k_2, k_3$ , and a local oscillator (LO) beams. The  $k_1, k_2$ , and  $k_3$  pulses were focused onto the sample with a 51 mm focal length gold-coated off-axis parabolic reflector. The phase-matching conditions for the dual-frequency experiments lead to a trapezoid spot pattern in the plane crossing the beams after the sample cell so that the beams with higher frequency hit the trapeze shorter-base corners. The thirdorder signal generated in the sample was picked at the phasematching direction  $(-k_1+k_2+k_3)$  by another parabolic reflector and mixed with the LO on an HgCdTe detector (Infrared Associates). The time delays,  $\tau$ , T, and t, between the  $k_1$  and  $k_2$ ,  $k_2$  and  $k_3$ , and  $k_3$  and LO pulses, respectively, [Fig. 1(g)] were controlled by the linear-motor-driven translation stages (Physik Instrumente). The spectra of the pulses were accurately measured and the relative intensities at various wavelengths were corrected for the monochromator dispersion.

The 2D data sets,  $I(t,\tau)$ , were recorded in the time domain and double Fourier transformed to obtain the 2D spectra,  $S(\omega_t, \omega_\tau)$ . Rephasing experiments were measured at different waiting times, T. The polarizations of all four beams

were kept vertical in this study, controlled by pairs of a half-wave plate (Karl Lambrecht Corp.) and a BaF<sub>2</sub> wire-grid polarizer (Specac Inc.). The scan length in 2DIR spectra depended on the transition accessed; it was 1.6, 1.1, and 2.6–2.8 ps for the CN, CO and Am-I, and the modes in the fingerprint region, respectively. The steps along the  $\tau$  and t directions were 5–8 ps, where larger steps were used for the lower-frequency transitions.

Dual-frequency heterodyned spectra,  $S(\omega_t, T)$ . For speedy acquisition of the cross-peak amplitude dependence on the waiting time T, we performed rephasing 2D I(t,T)photon-echo measurements, keeping  $\tau$  constant at ~130 fs. The scan length along t and the step were dependent on the transition accessed, similar to that in  $2DIR(\tau,t)$  measurements but ~20% longer; the number of laser shot accumulations per point was approximately two to three times larger (up to 500 per delay point in a data set). At least three data sets were acquired for the same cross peaks. These data sets were then Fourier transformed along the t direction resulting in the two-dimensional,  $S(\omega_t, T)$ , spectra. The T-dependence of a cross-peak amplitude was obtained by numerical integration of the absolute value  $S(\omega_t, T)$  along  $\omega_t$  in the window that selects the respective cross peak. The integration window cutoff limits were set to include points that have the amplitude greater than  $\sim 0.2$  of the maximal peak amplitude. Note that a peak in the one-dimensional  $\omega_t$  spectrum has contributions from all the peaks seen at the same  $\omega_t$  frequency in the 2D  $(\omega_t, \omega_\tau)$  spectrum measured in the same experimental conditions as it is essentially the projection of the two-dimensional spectrum onto the  $\omega_t$  axis. These measurements allow fast detection of the cross-peak amplitude as a function of waiting time, T, but are easily treatable when only a single mode is accessed by the  $k_1$  and  $k_2$  pulses. In case the  $k_1$  and  $k_2$  pulses excite more than one transition, the three-dimensional (3D) data sets,  $I(\tau,t,T)$ , were measured to detect the cross-peak-amplitude waiting-time dependence.

Two parameters were extracted from each cross-peak-amplitude T-dependence corrected to eliminate orientational motion:<sup>24</sup> The arrival time, which is the time at which the curve reaches its maximum, and the amplification coefficient, which is the ratio of the amplitudes at the maximum and at T=0. For accurate determination of the arrival times the cross-peak-amplitude T-dependences were fitted with a two-exponential function,  $A_0 + A_1 e^{-k_1 T} + A_2 e^{-k_2 T}$ .

SCHEME 1. Sketch of the PBN compound. The transition moment directions of three high-frequency modes are shown with arrows.

Quantum calculations. To help in the mode assignment, series of density functional theory (DFT) harmonic calculations were performed at Tulane's Center for Computational Science, using the GAUSSIAN 03, revision D.02, software. The best agreement with the experimental spectrum was obtained using the B3LYP functional and the 6-311++G(d,p) basis set.

#### **RESULTS AND DISCUSSION**

CN/Am-I and CN/CO cross peaks. The PBN compound chosen to test the potential of the RA 2DIR method has three convenient and mostly localized high-frequency modes, C ■N (CN), amide I (Am-I), and C=O (CO) (Scheme 1). The CN and amide groups are separated by  $\sim$ 6.5 Å and the direct CN/Am-I mode coupling is expected to be easily measurable. Indeed, the dual-frequency 2DIR measurements revealed a strong CN/Am-I cross peak derived from this interaction [Fig. 2(a)]. The linear spectrum of the PBN compound and the spectra of laser pulses used to measure 2DIR spectra are shown on the panels attached to the 2DIR spectra. The cross peak in Fig. 2(a) reflects the direct CN/Am-I mode coupling because the waiting time, T, was close to zero. As expected, the CN/CO cross peak in the spectrum measured at small delays T was diminutive [Fig. 2(a)], as the direct coupling between the CN and CO modes is very small. The small transition dipole of the CN mode<sup>25</sup> and large distance between the groups (>9 Å) makes the through space (electric) coupling negligible. The mechanical (through bond) coupling for this pair, while dominant over the electric coupling, is also expected to be small as the through-bond distance between the groups is large ( $\sim$ 11 Å). Note that the small feature that is seen close to the position where the CN/CO cross peak is expected is actually due to a ringing effect observed in the vicinity of the main CN/Am-I peak

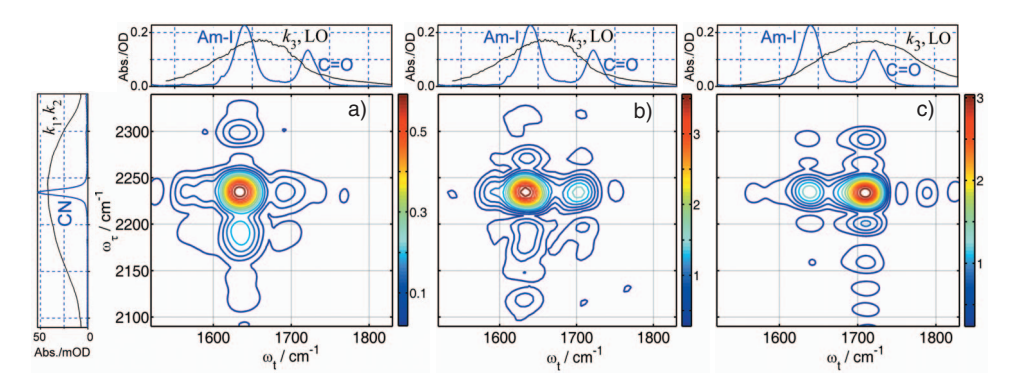


FIG. 2. (Color) Absolute-value dual-frequency 2DIR rephasing spectra of the PBN compound, at T=0.6 ps (a), T=10 ps (b), and T=10 ps (c). The linear spectrum of the PBN compound and the spectra of IR pulses used in each experiment are shown on the attached panels.

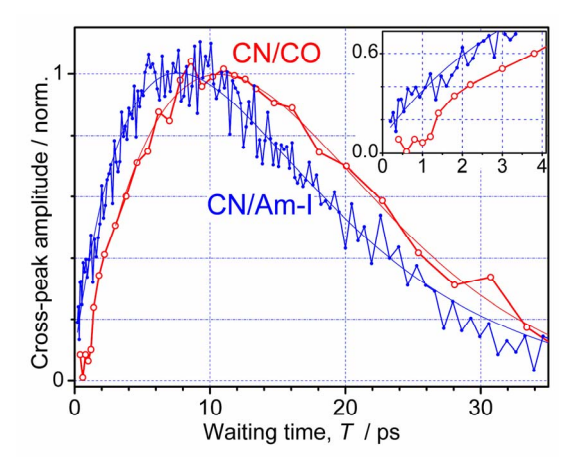


FIG. 3. (Color online) Normalized absolute-value amplitudes of the CN/Am-I and CN/CO cross peaks for PBN compound as a function of time delay T. The thin smooth lines are the fits with a two-exponential function used to measure the peak position. Initial region for T < 4 ps is also shown in the inset. Note that the CN/Am-I and CN/CO cross peaks were measured using the pulses shown in Figs. 2(a) and 2(c), respectively.

(vide infra). Gratifyingly, the CN/CO cross peak is sizable in the RA 2DIR spectrum measured at T=10 ps [Fig. 2(b)]. In fact both cross peaks, CN/Am-I and CN/CO, are now much stronger than those in Fig. 2(a) [compare the color bars in Figs. 2(a) and 2(b)]. Moreover, the CN/CO cross peak could be selectively enhanced further by centering the  $k_3$  and LO pulse spectra at  $\omega_{\rm CO}$  frequency [Fig. 2(c)]. The CN/CO cross peak is now the dominant peak in the spectrum, despite the fact that the distance between the CN and CO groups is almost twice as large as the distance between the CN and amide groups.

The amplitudes of the two cross peaks were measured as a function of time delay, T, by acquiring 2D (t,T) spectra (Fig. 3). Both cross peaks grow substantially with the time delay, T. We found two parameters convenient for the discussion of differences in these two dependences. One is the time delay at which the curve reaches its maximum, the excess-energy arrival time, or just arrival time,  $T_{\text{max}}$ . The second parameter, the amplification coefficient,  $\gamma$ , is the ratio of the amplitudes at the maximum and at T=0. The CN/Am-I cross-peak amplitude reaches maximum at  $7.5 \pm 0.7$  ps and the amplification coefficient is  $4.3 \pm 0.6$ ; the respective values for the CN/CO cross peak are  $10.6 \pm 0.6$  ps and  $18 \pm 2$ (Fig. 3). One can see that there is a qualitative correlation between the arrival time and the intermode distance: for the pair of modes separated by smaller distance, CN-Am-I pair, the arrival time,  $T_{\rm max}$ , is smaller than that for the pair with larger distance, CN—CO. The amplification coefficient also correlates with the distance:  $\gamma$  is larger for larger intermode distances. The origin of the large amplification observed for the CN/CO cross peak is in a softer distance dependence of the energy transport efficiency compared to the direct-coupling distance dependence.<sup>21</sup> The distance dependence for the off-diagonal anharmonicity  $\Delta_{12}$  depends on the coupling mechanism. Electric coupling causes  $1/R^6$  distance dependence of  $\Delta_{12}$ . The distance dependence of mechanical coupling is less understood as it depends strongly on the type of bonds (the bridge) separating the two modes; an exponential decay of the off-diagonal anharmonicity is expected for the bridges featuring only single bonds. In a simplest model the RA cross-peak amplitude can be associated with the excess energy present at the  $\omega_2$  site after that was transferred from the  $\omega_1$  mode of the molecule (Fig. 1). The maximum cross-peak amplitude will be achieved when the excess energy at the  $\omega_2$  site reaches its maximum. The assumption that energy transport in a molecule can be treated as heat conduction in macromaterial leads to 1/R or  $1/R^2$ dependences for the maximal temperature that can be reached at distance R from the heat source for the case of one- and two-dimensional heat conduction scenarios, respectively. So drastically different distance dependences for the amplitudes of the direct and RA cross peaks lead to a conclusion that larger amplification factors are expected for larger distances between the modes.

The shape of the curve for the CN/CO cross peak in Fig. 3 has several interesting features. There is a clear induction period that lasts until  $T \sim 1.3$  ps, followed by a sharp amplitude increase (Fig. 3, inset). One would expect similar behavior if the process is described by a heat transport equation. These dependences, however, should be modeled in a more complex way because of two factors. First, the energy transport process at small delay times occurs in conditions that are far from being at local statistical equilibrium. 27-29 Second, there are several energy accepting modes that are coupled to the probed mode (including the  $\omega_2$  mode itself); the accepting-mode spatial locations are different and their coupling strengths with the probed mode are different. The sharp growth of the cross-peak amplitude that started at  $\sim$ 1.3 ps is probably associated with the modes that are substantially delocalized, can be quickly populated via CN relaxation, and also are much stronger coupled to the CO than the CN mode is. Note that the lifetime of the excited CN, CO, and Am-I modes are  $6.3 \pm 0.1$  ps,  $0.6 \pm 0.15$  ps, and  $0.85 \pm 0.15$  ps, respectively (see Scheme 1). At larger time delays. T, the excess energy travels further from the CN group, reaches the CO site, and populates the modes that reside on the same group of atoms as the CO mode, which ensures their strong mechanical coupling with the CO mode. The cross peak reaches maximum when this happens. The competing processes is the overall cooling of the molecule which causes the cross-peak amplitude decrease at times >12 ps. The characteristic time for the cooling process is  $\sim$ 20 ps (Fig. 3).

The RA 2DIR spectrum extended to the fingerprint region. Despite the difficulties in modeling of the cross-peak amplitude dependences on T, it seems that they, nevertheless, can be used for quick assessment of the relative intermode distances. To test this idea further, we have measured RA 2DIR cross peaks between the CN, CO, Am-I, and other modes of the PBN compound. The combined RA 2DIR spectrum measured at T=10 ps is shown in Fig. 4. The spectrum shows over 25 cross peaks from 11 vibrational modes, demonstrating the power of the RA 2DIR method and the power of the dual-frequency approach. The spectrum is merged from seven pieces, each being normalized independently. The assignment of some of the modes is clear and straightforward, such as for the CN, CO, Am-I, Am-II (1438 cm $^{-1}$ ),

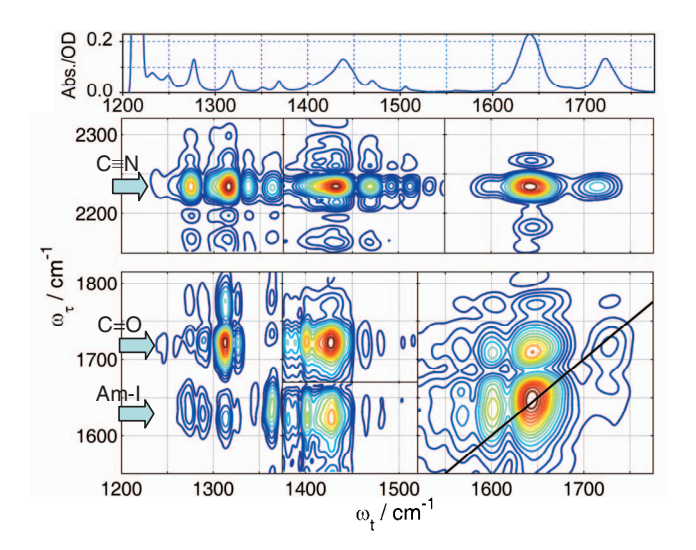


FIG. 4. (Color) Dual-frequency RA 2DIR rephasing absolute-value spectrum of the PBN compound measured at T=10 ps and merged from seven parts, each part being normalized independently, except the spectrum at the bottom of the middle section, for which the amplitude relation with the section above is preserved. The linear spectrum of the PBN compound is shown in the upper panel. Three arrows at the left at CN, CO, and Am-I frequencies indicate  $\omega_t$  frequencies at which the reliable cross peaks are located. The weaker peaks at different  $\omega_\tau$  frequencies are caused by ringing artifacts. The origin of the cross peak at (1480, 2235 cm<sup>-1</sup>) is unclear.

and phenyl ring stretches (1506 cm<sup>-1</sup>). It is more difficult to assign transitions between 1250 and 1470 cm<sup>-1</sup> as most of them are delocalized over multiple bonds and have contributions from bending, wagging, and scissoring motion of CH<sub>2</sub> and/or CH groups which was confirmed by the DFT calculations performed using GAUSSIAN 03 software. <sup>30</sup> We now analyze the predictions of the RA 2DIR approach on the spatial location of the modes. The dependences of the crosspeak amplitudes on the time delay, T, for several cross peaks are shown in Fig. 5. The left panel presents the dependences for the cross peaks between CN and five other modes; the corresponding cross peaks appear in Fig. 4 on the line  $\omega_t$ 

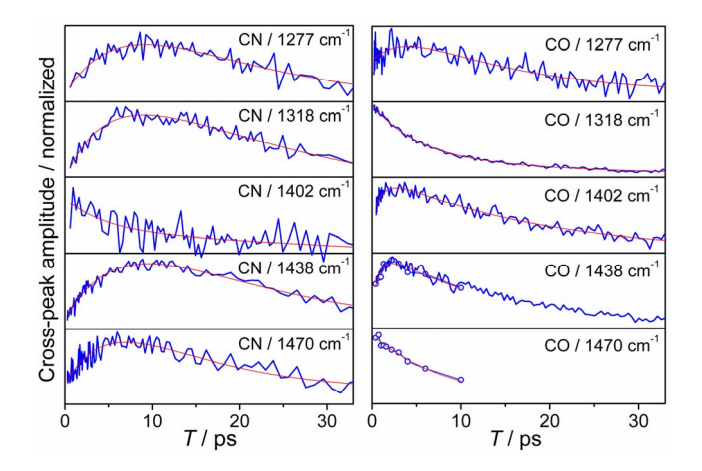


FIG. 5. (Color online) Normalized cross-peak amplitudes as a function of time delay, T, measured for various mode pairs with zzzz beam polarizations. Left panel: CN mode excitation; right panel: CO mode excitation. The data shown by thick noisy lines were obtained from (t,T) 2D spectra; the circles on the right panel represent amplitudes measured from the  $(\tau,t,T)$  3D spectra. The thin smooth lines are the fits with a two-exponential function used to determine peak positions.

=2234 cm<sup>-1</sup>. As seen from the graphs, different cross peaks have different arrival times and different amplification coefficients which are summarized in Table I. For example, the modes at 1402 and 1506 cm<sup>-1</sup> have contributions from the phenyl ring C—C stretches (DFT calculations). As they are spatially close to the CN group, their direct couplings with the CN mode are substantial, resulting in decays of the crosspeak amplitudes as a function of waiting time, T. On the contrary, the amide-II mode (Am-II, 1438 cm<sup>-1</sup>), which involves mostly C—N stretching motion in the amide, is far from the CN group and the CN/Am-II cross peak exhibiting the arrival time of  $9.0 \pm 0.6$  ps and amplification coefficient of  $5.4 \pm 0.4$ . One can say that it takes about 9 ps for excess energy to travel from the initially excited CN mode to the site where Am-II mode is located.

Interestingly, the arrival time and amplification coefficient for the CN/Am-II cross peak, 9.0 ps and 5.4, are larger than those for the CN/Am-I peak,  $7.5 \pm 0.5$  ps and  $4.3 \pm 0.4$ , despite similar CN—Am-I and CN—Am-II distances. Due to different spatial locations of Am-I and Am-II modes, the lower-frequency modes strongly coupled to them will have different locations as well: Those coupled to the Am-I are located more on the phenyl-ring side of the amide while those coupled to the Am-II mode are mostly located on the piperidine-ring side of the amide. We suggest that different  $T_{\rm max}$  values for the CN/Am-I and CN/Am-II cross peaks (by 1.5 ps) are observed mostly because different accepting modes are involved for the two cross peaks. This observation supports the hypothesis that the largest contribution to the cross-peak amplification is obtained when the excess energy reaches not the mode that is probed (Am-I or Am-II) but some lower-frequency modes that are coupled to the probed mode. Note that due to their high frequencies the probability of having Am-I or Am-II mode excited after  $\sim 5-7$  ps of the cooling process is expected to be small. 31-33 The amplification coefficient values for these mode pairs agree with the  $T_{\rm max}$  values: Larger amplification coefficient is measured for the pair that requires longer energy transport. Surprisingly, the arrival time for the CN/CO cross peak is only 1.6 ps larger than that for the CN/Am-II cross peak. This confirms that the energy accepting modes that are strongly coupled to the Am-II mode are located on the atoms of the amide and piperidine ring. It also suggests that the piperidine ring transmits energy efficiently and after the modes on the amide side of the ring are excited it takes only a small extra time to propagate across the ring and reach the CO site. Due to the symmetry of the ring and large number of degenerate modes, most of the normal modes in the ring are delocalized. Such modes are expected to transfer energy efficiently, <sup>28,29</sup> as observed experimentally in these measurements.

It is instructive to compare the energy transport in the PBN molecule originated from different starting sites (modes). Figure 5 shows the side-by-side comparison of the cross-peak amplitude dynamics when the initially excited modes were the CN (left panel) and CO (right panel) modes. The  $T_{\rm max}$  and  $\gamma$  values for the CN, CO, and Am-I–excited cross peaks are shown in Table I; the  $T_{\rm max}$  values are also shown schematically in Fig. 6. Approximate additivity of the arrival times is observed for several modes (1277, 1369,

TABLE I. The arrival time ( $T_{\text{max}}$ ) and amplification coefficient ( $\gamma$ ) measured for three groups of cross peaks with  $\omega_r$  equals 2234 cm<sup>-1</sup> (CN excitation), 1722 cm<sup>-1</sup> (CO excitation), and 1640 cm<sup>-1</sup> (Am-I excitation).

$\omega_t \text{ (cm}^{-1})$	$\omega_r = 2234 \text{ cm}^{-1}$ (CN excitation)		$\omega_r = 1722 \text{ cm}^{-1}$ (CO excitation)		$\omega_r = 1640 \text{ cm}^{-1}$ (Am-I excitation)	
	$T_{\rm max}^{\rm f}$ (ps)	γ	$T_{\max}^{f}$ (ps)	γ	$T_{\rm max}^{\rm f}$ (ps)	γ
1277	9.5 ± 1.5	$5.0 \pm 1.0$	$3.5 \pm 1.0$	$1.6 \pm 0.4$	O <sup>a</sup>	1
1318	$8.8 \pm 1.5$	$4.6 \pm 0.9$	0	1	$2.1 \pm 0.4$	$1.4 \pm 0.2$
1369	$9.5 \pm 1.6$	$4.5 \pm 1.3$	0	1	$2.0 \pm 0.4^{b}$	1-1.03
1402	0	1	$2.5 \pm 0.6$	$1.4 \pm 0.2$	0	1
1438 (Am-II)	$9.0 \pm 0.6$	$5.4 \pm 0.4$	$2.4 \pm 0.4$	$1.7 \pm 0.2$	$1.9 \pm 0.2^{b}$	1
1470	$6.6 \pm 1.1$	$2.6 \pm 0.4$	0	1	c	
1506	0	1	d		c	
1609	d	•••	$4.5 \pm 0.8$	1.5–3 <sup>e</sup>	0	1
1640 (Am-I)	$7.5 \pm 0.7$	$4.3 \pm 0.6$	$3.5 \pm 0.6$	1.5–3 <sup>e</sup>		
1722 (CO)	$10.6 \pm 0.6$	$18 \pm 2$				

<sup>&</sup>lt;sup>a</sup>The cross-peak amplitude decreases as a function of the delay time, T.

1438, and 1640 cm<sup>-1</sup>). For example, it takes 10.6 ps for the energy to cross the molecule from the CN to CO modes and it takes 7.5 ps to reach Am-I from CN and 3.5 ps to reach Am-I from CO, which amounts at ~11 ps for the time to cross the whole molecule (Table I). Also, it takes 9 ps to reach Am-II from CN and 2.3 ps to reach Am-II from CO, with the total time to cross the whole molecule of ~11.3 ps, which is again close to the CN/CO arrival time of 10.6 ps. Although more experiments are needed to test different cases

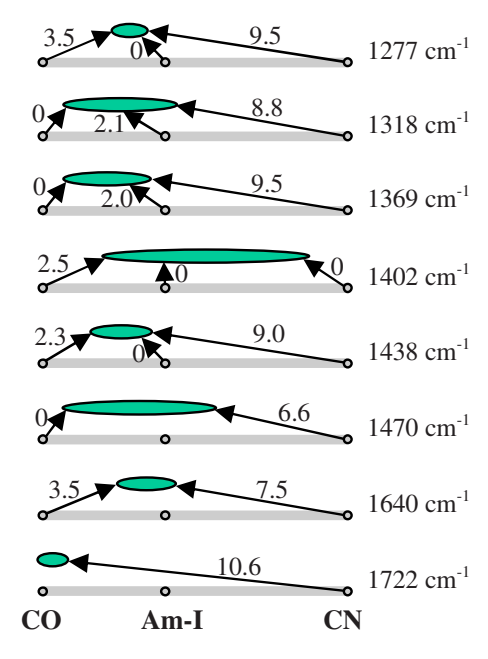


FIG. 6. (Color online) Schematic representation of the experimental data (see text). The arrows represent energy transport initiated by excitation of one of the modes, CN, Am–I, or CO. The numbers by the arrows are the arrival times in picoseconds for the modes shown at the right.

and understand various factors that affect the arrival times, such monotonic correlation between the distance and the arrival time is encouraging and brings an opportunity of using RA 2DIR method for accessing the bond connectivity patterns in molecules.

Some other modes, especially those at 1402 and 1470 cm<sup>-1</sup>, do not show such apparent additivity but exhibit the arrival times which suggest that these modes are close to both ends of the molecule (Table I). This is possible only if the modes are strongly delocalized over multiple bonds. As a working hypothesis we suggest that the size of delocalization can be estimated using RA 2DIR technique. For example, the mode at 1402 cm<sup>-1</sup> has a contribution of the C-C stretching motion in the phenyl ring (DFT calculations). As the phenyl ring is spatially close to the CN group, no amplification of the CN/1402 cross peak is observed (Fig. 5). The  $T_{\rm max}$ value for the CO/1402 cross peak (2.5 ps) is smaller than that for the CO/Am-I cross peak (3.5 ps) suggesting also that the 1402 cm<sup>-1</sup> mode has a contribution on the piperidine ring. The assignment of the mode at 1470 cm<sup>-1</sup> is less certain. The closest calculated normal mode is at 1490 cm<sup>-1</sup> which, using a typical scaling factor of 0.98, falls at 1460 cm<sup>-1</sup>. Atom displacement patterns of the normal modes of interest are given in the Supplementary Materials (Fig. S4).

The arrival times obtained with Am-I mode excitation support further the data on the mode delocalization. For example, based on the data for the CN/1402 and CO/1402 cross peaks we argue that the 1402 cm<sup>-1</sup> mode is delocalized over the phenyl ring and the amide group. The  $T_{\rm max}$ =0 for the Am-I/1402 cross peak suggests a presence of the 1402 cm<sup>-1</sup> mode somewhere on the amide group supporting its large delocalization. The predictions of mode delocalization ob-

<sup>&</sup>lt;sup>b</sup>A plateau is observed until the time shown.

<sup>&</sup>lt;sup>c</sup>Strong Am-I/Am-II cross peak prevents accurate measurements.

<sup>&</sup>lt;sup>d</sup>The cross peak is too weak to measure.

<sup>&</sup>lt;sup>c</sup>Strong diagonal peaks prevent accurate measurements of  $\gamma$ . Note that at larger T-delays the diagonal contribution decreases while the RA cross-peak contribution increases, permitting accurate measurements of  $T_{\text{max}}$ .

fThe  $T_{\rm max}$  and  $\gamma$  values were determined from reconstructed magic-angle T-dependences of the cross-peak amplitude performed using the known angles between transition dipoles for several mode pairs. (Refs. 35 and 36) such as CN/CO ( $\sim$ 60°), CN/Am-II (60°–70°), CN/Am-II (60°), CO/Am-II (50–60°), and CO/Am-II (50–60°), see Supplementary Materials. For other mode pairs with unclear transition moment directions two magic-angle data sets were computed assuming 0° and 90° angles between the transition moments. The deviations in  $T_{\rm max}$  and  $\gamma$  parameters obtained from these limiting cases were incorporated into their error bars. Note that for all cross peaks the error bars associated with orientation motion were less than 10% for both  $T_{\rm max}$  and  $\gamma$  parameters.

tained by the RA 2DIR method are schematically summarized in Fig. 6. The thick gray horizontal lines symbolize the molecular skeleton with CO and CN groups located at the left and right sides, respectively. The arrival times are shown by arrows with lengths proportional to the arrival time values. The arrows start from the group where the initially excited mode is located. For example, the top scheme shows the arrival times for the mode at 1277 cm<sup>-1</sup>, when CO, Am-I, and CN modes were initially excited; the corresponding arrival times for the CO/1277, Am-I/1277, and CN/1277 cross peaks are 3.5, 0, and 9.5 ps. The ovals in Fig. 6 show qualitatively the delocalization sizes for the respective modes and how they appear from the RA 2DIR data. Further experiments will clarify the capability of the method in making quantitative predictions on the mode delocalization. It is well known that the extent of mode delocalization strongly depends on the molecular structure.<sup>34</sup> The ability of RA 2DIR in measuring the sizes of delocalization is not only providing an access to important molecular characteristic but may lead to a new type of reporters in structural measurements.

#### SUMMARY

We have experimentally demonstrated that the bond connectivity patterns can be measured using the RA 2DIR method. The energy arrival time and the amplification factor are shown to be convenient parameters for analyzing the bond connectivities. The correlation of the arrival time and the intermode distance has been experimentally detected on multiple mode pairs. The mean rate of the energy transport of  $\sim$ 1 Å/ps, measured in PBN, appeared to be  $\sim$ 15-fold slower than the speed of sound in water,  $\sim 15 \text{ Å/ps}$ . It is expected that the arrival time will be affected by several factors, such as the nature of the modes, the structure and identity of the bonds connecting the two modes, and possibly the interactions with the solvent or surroundings. To achieve predictive power in correlating the  $T_{\rm max}$  and  $\gamma$  values with the intermode distance, a detailed modeling of the T-delay dependence of the cross-peak amplitudes is needed.

The large amplification of the cross-peak amplitude (~18-fold) shown in this work enhances the applicability of 2DIR spectroscopy by permitting the long-range measurements and measurements using weak IR modes. With a proper calibration, the RA 2DIR method is expected to permit speedy assessments of the bond connectivity patterns and distances, which indicates an analytical potential of the method.

### **ACKNOWLEDGMENTS**

The support by Louisiana Board of Regents via RCS and Enhancement grants is gratefully acknowledged.

- <sup>2</sup>M. C. Asplund, M. T. Zanni, and R. M. Hochstrasser, Proc. Natl. Acad. Sci. U.S.A. 97, 8219 (2000).
- <sup>3</sup> J. B. Asbury, T. Steinel, and M. D. Fayer, J. Phys. Chem. B 108, 6544 (2004).
- <sup>4</sup>S. Woutersen, Y. Mu, G. Stock, and P. Hamm, Proc. Natl. Acad. Sci. U.S.A. 98, 11254 (2001).
- <sup>5</sup>C. Fang and R. M. Hochstrasser, J. Phys. Chem. B 109, 18652 (2005).
- <sup>6</sup>N. Demirdoven, C. M. Cheatum, H. S. Chung, M. Khalil, J. Knoester, and A. Tokmakoff, J. Am. Chem. Soc. 126, 7981 (2004).
- <sup>7</sup>J. Bredenbeck, J. Helbing, A. Sieg, T. Schrader, W. Zinth, C. Renner, R. Behrendt, L. Moroder, J. Wachtveit, and P. Hamm, Proc. Natl. Acad. Sci. U.S.A. 100, 6452 (2003).
- <sup>8</sup>P. Mukherjee, A. T. Krummel, E. C. Fulmer, I. Kass, I. T. Arkin, and M. T. Zanni, J. Chem. Phys. **120**, 10215 (2004).
- <sup>9</sup>M. Khalil, N. Demirdoven, and A. Tokmakoff, J. Chem. Phys. **121**, 362 (2004).
- <sup>10</sup> F. Ding, E. C. Fulmer, and M. T. Zanni, in *Springer Series in Chemical Physics*, edited by P. Corkum, D. M. Jonas, R. J. D. Miller, and A. M. Weiner (Springer, New York, 2006), Vol. 88, p. 404.
- <sup>11</sup> I. V. Rubtsov, J. Wang, and R. M. Hochstrasser, Proc. Natl. Acad. Sci. U.S.A. **100**, 5601 (2003).
- <sup>12</sup> I. V. Rubtsov, K. Kumar, and R. M. Hochstrasser, Chem. Phys. Lett. **402**, 439 (2005).
- <sup>13</sup> D. V. Kurochkin, S. G. Naraharisetty, and I. V. Rubtsov, J. Phys. Chem. A **109**, 10799 (2005).
- <sup>14</sup>C. Scheurer and S. Mukamel, J. Chem. Phys. **116**, 6803 (2002).
- <sup>15</sup> K. Kumar, L. E. Sinks, J. Wang, Y. S. Kim, and R. M. Hochstrasser, Chem. Phys. Lett. **432**, 122 (2006).
- <sup>16</sup>R. M. Hochstrasser, Adv. Chem. Phys. **132**, 1 (2006).
- <sup>17</sup> R. R. Ernst, G. Bodenhausen, and A. Wokaun, *Principles of Nuclear Magnetic Resonance in One and Two Dimensions* (Oxford University Press, New York, 1987).
- <sup>18</sup> A. E. Derome, Modern NMR Techniques for Chemistry Research (Pergamon, New York, 1997).
- <sup>19</sup>S. G. Naraharisetty, D. V. Kurochkin, and I. V. Rubtsov, Chem. Phys. Lett. **437**, 262 (2007).
- <sup>20</sup> D. V. Kurochkin, S. G. Naraharisetty, and I. V. Rubtsov, in *Springer Series in Chemical Physics*, edited by P. Corkum, D. M. Jonas, R. J. D. Miller, and A. M. Weiner (Springer, New York, 2006), Vol. 88, p. 344.
- <sup>21</sup> D. V. Kurochkin, S. G. Naraharisetty, and I. V. Rubtsov, Proc. Natl. Acad. Sci. U.S.A. **104**, 14209 (2007).
- <sup>22</sup> J. Dreyer, A. M. Moran, and S. Mukamel, J. Phys. Chem. B **107**, 5967 (2003).
- <sup>23</sup>C. P. Lawrence and J. L. Skinner, Proc. Natl. Acad. Sci. U.S.A. 102, 6720 (2005).
- <sup>24</sup> See EPAPS Document No. E-JCPSA6-128-009809 for more details. This document can be reached through a direct link in the online article's HTML reference section or via the EPAPS homepage (http://www.aip.org/pubservs/epaps.html).
- <sup>25</sup> Z. Getahun, C.-Y. Huang, T. Wang, B. De Leon, W. F. DeGrado, and F. Gai, J. Am. Chem. Soc. **125**, 405 (2003).
- <sup>26</sup> P. Hamm and R. M. Hochstrasser, in *Ultrafast Infrared and Raman Spectroscopy*, edited by M. D. Fayer (Dekker, New York, 2000), p. 273.
- <sup>27</sup>M. Gruebele and P. G. Wolynes, Acc. Chem. Res. **37**, 261 (2004).
- <sup>28</sup>D. M. Leitner, Adv. Chem. Phys. **130B**, 205 (2005).
- <sup>29</sup> H. Fujisaki, Y. Zhang, and J. E. Straub, J. Chem. Phys. **124**, 144910 (2006)
- <sup>30</sup> M. J. Frisch, G. W. Trucks, H. B. Schlegel *et al.*, GAUSSIAN 03, Revision D.02, Gaussian, Inc., Wallingford, CT, 2004.
- <sup>31</sup>I. V. Rubtsov and R. M. Hochstrasser, J. Phys. Chem. B **106**, 9165 (2002)
- <sup>32</sup>Z. Wang, A. Pakoulev, and D. D. Dlott, Science **296**, 2201 (2002).
- <sup>33</sup> J. C. Deak, Y. Pang, T. D. Sechler, Z. Wang, and D. D. Dlott, Science 306, 473 (2004).
- <sup>34</sup>H. Torii and M. Tasumi, J. Chem. Phys. **96**, 3379 (1992).
- <sup>35</sup> S. Krimm and J. Bandekar, Adv. Protein Chem. **38**, 181 (1986).
- <sup>36</sup> W. H. Moore and S. Krimm, Biopolymers **15**, 2439 (1976).

<sup>&</sup>lt;sup>1</sup>P. Hamm, M. Lim, and R. M. Hochstrasser, J. Phys. Chem. B **102**, 6123 (1998).